Hindawi
Journal of Sensors
Volume 2023, Article ID 9753429, 1 page
https://doi.org/10.1155/2023/9753429

Retraction

Retracted: A Training Method for a Sensor-Based Exercise Rehabilitation Robot

Journal of Sensors

Received 3 October 2023; Accepted 3 October 2023; Published 4 October 2023

This article has been retracted by Hindawi following an investigation undertaken by the publisher [1]. This investigation has uncovered evidence of one or more of the following indicators of systematic manipulation of the publication process:

(1) Discrepancies in scope
(2) Discrepancies in the description of the research reported
(3) Discrepancies between the availability of data and the research described
(4) Inappropriate citations
(5) Incoherent, meaningless and/or irrelevant content included in the article
(6) Peer-review manipulation

The presence of these indicators undermines our confidence in the integrity of the article's content and we cannot, therefore, vouch for its reliability. Please note that this notice is intended solely to alert readers that the content of this article is unreliable. We have not investigated whether authors were aware of or involved in the systematic manipulation of the publication process.

Wiley and Hindawi regrets that the usual quality checks did not identify these issues before publication and have since put additional measures in place to safeguard research integrity.

We wish to credit our own Research Integrity and Research Publishing teams and anonymous and named external researchers and research integrity experts for contributing to this investigation.

The corresponding author, as the representative of all authors, has been given the opportunity to register their agreement or disagreement to this retraction. We have kept a record of any response received.

References

[1] P. Suo, X. Zhu, S. Wang et al., "A Training Method for a Sensor-Based Exercise Rehabilitation Robot," *Journal of Sensors*, vol. 2022, Article ID 4336664, 9 pages, 2022.

Hindawi
Journal of Sensors
Volume 2022, Article ID 4336664, 9 pages
https://doi.org/10.1155/2022/4336664

Research Article

A Training Method for a Sensor-Based Exercise Rehabilitation Robot

Peng Suo,[1] **Xueqiang Zhu**,[1] **Shu Wang**,[2] **Mei Li**,[1] **Ting Yu**,[1] **Chunning Song**,[1] **Haodi Ning**,[3] **and Yi Xin**[4]

[1]*Shandong Sport University, Jinan, Shandong 250102, China*
[2]*Shandong Sports Rehabilitation Research Center, Jinan, Shandong 250102, China*
[3]*Shandong Taishan Football Club Co., Ltd, Jinan, Shandong 250102, China*
[4]*Shandong Sport Science Research Center, Jinan, Shandong 250102, China*

Correspondence should be addressed to Yi Xin; 1710200415@hbut.edu.cn

Received 22 June 2022; Revised 14 July 2022; Accepted 23 July 2022; Published 2 August 2022

Academic Editor: Haibin Lv

In order to solve the problem that the traditional mirror therapy did not take into account the real-time recovery of the affected limb and the training effect was limited, a training method of sports rehabilitation robot based on sensor was proposed. A mirror active rehabilitation training system was proposed, which was composed of four steps including trajectory acquisition of the limb inertial measurement unit (IMU), fuzzy adaptive proportion differentiation (PD) control in closed-loop variable domain, muscle force estimation of the surface electromyographic signal (sEMG) of the affected limb, and power compensation of the outer ring of the affected limb. The experimental results showed that the sagittal forward flexion angle of the healthy shoulder increased from 0° to 128° at a relatively uniform speed, and the sagittal forward flexion angle of the shoulder was basically consistent with that of the healthy limb after the adaptive power compensation of the affected limb. The calculated trajectory tracking error of the healthy limb controlled by the fuzzy adaptive PD controller in the variable domain was $0.21 \pm 1.35°$. The horizontal backward extension angle of the healthy shoulder joint increased from 0° to 43°, and the following trajectory of the affected limb was roughly consistent with the movement trajectory of the healthy limb. The calculated tracking error of the healthy limb trajectory was $0.39 \pm 1.45°$. It was concluded that the control system could provide the real-time power compensation according to the recovery of the affected limb, give full play to the training initiative of the affected limb, and make the affected limb achieve a better rehabilitation training effect.

1. Introduction

Sports injury refers to a variety of injuries that may occur when people are exercising. These sports injury reason mainly includes personal internal factors and external environment factors. The personal internal factors include exercise without warming up, lack of basic training, movement against science movement principle, incorrect movement posture, and a bad sports competitive state. The external environment factors include lack of scientific guidance of movement, without wearing special clothing, the improper organization of the training and competition, and the poor climate [1]. With the continuous pursuit of the quality of life, the public's health awareness has gradually improved. More and more people began to improve their physical fitness through a variety of sports and exercise. But it is followed by a variety of sports injuries, bringing pain to people and affecting the normal work and study. At the same time, the proportion of sports injury in sports competition is higher. The survey found that national snowboarders had a 70% probability of some degree of sports injury during their career. In addition, once an athlete is injured, he or she cannot normally participate in the training and competition in a short period of time, and his or her psychology will also be affected. The double injury of physical and psychological will seriously affect the performance of the competition [2].

For different types of sports, the corresponding types and proportion of sports injuries are also different. The common types of sports injuries mainly include the acute injuries, such

as muscle strain, ligament injury, and fracture, or the chronic injuries such as tenosynovitis, bursitis, fatigue fracture, and muscle spasm. In the process of the injury rehabilitation, the sports treatment technology has played an important role. The exercise therapy technology is based on the biological mechanics, kinematics, and neurology, and blood circulation and metabolism of the body's tissues are improved in the form of the passive or active movement, so as to improve the damaged muscle strength and endurance and speed up the recovery of neural function, cardiopulmonary function, and the balance ability. Clinical practice has found that regular and periodic rehabilitation exercise can effectively accelerate the rehabilitation process, and the rehabilitation effect is better [3]. The scientific rehabilitation training can not only improve joint range of motion, improve muscle strength, and improve body coordination but also prevent muscle atrophy, osteoporosis, and other diseases, as shown in Figure 1.

2. Literature Review

Baothman and Edhah proposed the CPC model. Two parameters were added to the traditional D-H model, and the added parameters are used to realize the continuity of the robot kinematics model. The core was to define six parameters for each link of the robot to represent the rotation of the robot. This modeling method emphasized the integrity and continuity of parameters and solved the defects of traditional D-H models to a certain extent. This model was also improved in later experiments, and a new modeling method was proposed, called MCPC model [4]. Medghalchi et al. constructed POE model based on screw theory. In the model, only the inertial coordinate system and the tool coordinate system were determined during the system construction, which improved the modeling efficiency. In the calibration process, the modeling method did not need to identify the joint zero error separately, which simplified the calculation and improved the calibration efficiency. At the same time, the method also overcame the singularity problem in the traditional D-H model [5]. Yang et al. found that mirror therapy had a significant effect on patients with nerve injury and poor motor function [6]. Loflin et al. performed mirror therapy on stroke patients and found that the active range of motion and motor speed in the treated group were improved compared with those in the untreated group [7]. Tsoi et al. confirmed that mirror therapy had an obvious effect on weakening the pain sensation of the affected limb [8].

The traditional mirror rehabilitation training method has achieved a good effect in improving the motor ability of patients, but in the traditional therapy, the affected side does not get the actual rehabilitation training exercise. In order to avoid the disadvantages of traditional mirror therapy to a certain extent, a rehabilitation therapy was proposed, which integrated the mirror idea of the healthy limb movement into the robot system. Liu et al. used inertial measurement unit (IMU) to map the joint space motion trajectory of the healthy limb to the exoskeleton of the affected limb for synchronous mirror motion, which improved the rehabilitation effect of patients [9]. Vicharapu et al. developed a virtual reality mirror training system with Kinect and exoskeleton, which could detect the movement intention of rehabilitation robot. Experiments showed that this system could be widely used as a therapeutic intervention method. Many researches showed that it had excellent therapeutic effects when the patients received the rehabilitation training on their healthy limbs at the same time [10].

The above mirror therapy realized the rehabilitation training of the affected limb through the synchronous mirror movement of the affected limb and the healthy limb assisted by the rehabilitation robot. However, it is just a simple passive following training, without considering the real-time recovery of the affected limb. So the training effect is limited. In order to solve the problem, an adaptive control method of mirror rehabilitation training is proposed. By constructing shoulder joint dynamics model and muscle force estimation model to calculate the compensation moment of the affected limb, the method can provide real-time power compensation for the affected limb to improve the initiative of the training of the affected limb, realizing the maximum training of muscle strength of the affected limb in the process of mirror training.

3. Research Methods

3.1. Structural Design of the Shoulder Rehabilitation Robot. According to the biomechanical characteristics of human shoulder joint, shoulder joint is composed of clavicle, humerus, and scapula, which is a typical ball and socket joint and can carry out multiaxial flexible movement. Shoulder joint motion can be specifically decomposed into three orthogonal motions: abduction or adduction in the coronal plane, flexion or extension in the sagittal plane, and internal rotation or external rotation in the horizontal plane [11].

According to the above biomechanical decomposition of human shoulder motion, an exoskeleton shoulder rehabilitation robot was developed in the research. Three orthogonal revolute joints J1, J2, and J3 in series were used to realize the ball joint motion of shoulder. At the same time, in order to meet the sitting height of different people, the robot was designed to be fixed on the lifting base. The whole structure could meet the needs of different body types.

3.2. Adaptive Adjustment Assisted Control Algorithm Design of Mirror Rehabilitation Training. In order to maximally train the muscle strength of the affected limb in the mirror rehabilitation training, the above exoskeleton-type shoulder rehabilitation robot was used as the experimental platform, and an adaptive adjustment assisted mirror rehabilitation training control method was proposed. It is mainly composed of four parts including the limb trajectory acquisition based on IMU, fuzzy adaptive proportion differentiation (PD) control in variable domain, muscle force estimation of affected limb based on surface electromyography, and adaptive power adjustment of the affected limb [12].

3.2.1. The Healthy Limb Trajectory Acquisition Based on IMU. In this system, IMU was used to capture the motion track of shoulder joint of healthy limb. Here, the original information provided by IMU needs to be converted to the shoulder coordinate system. The IMU was worn on the inner side of the

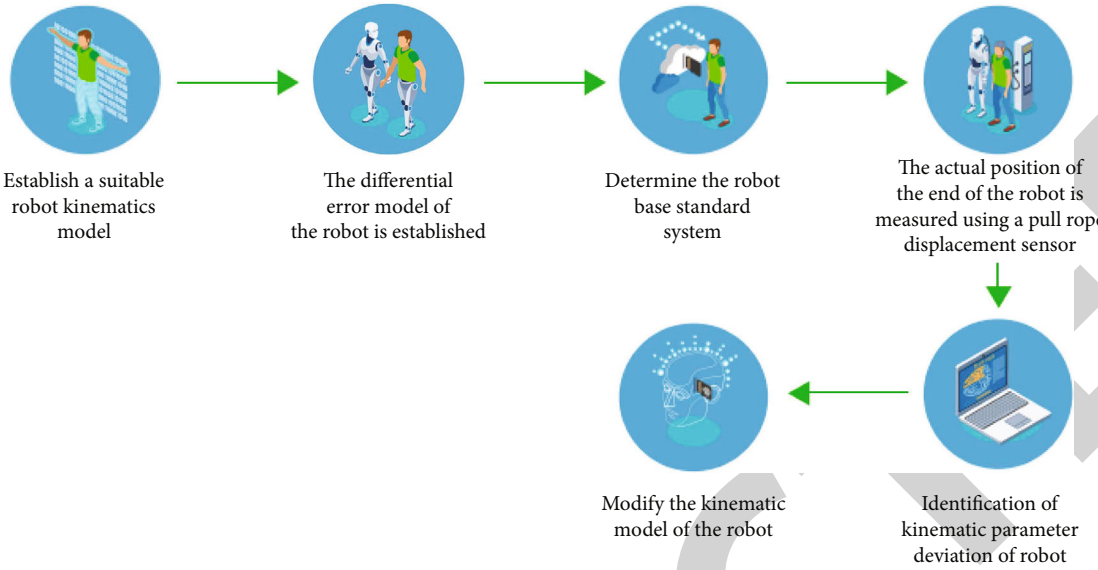

Figure 1: Sports rehabilitation robot training method.

upper arm, and the coordinates of IMU were set as O_{uvw} and shoulder joint as O_{xyz}.

All relevant original coordinate data joints can obtain new position vectors through rotation matrix R^T, which can be obtained as follows. Suppose that O_{xyz} has a fixed point M, and its position vectors at O_{uvw} and O_{xyz} are P_M^{uvw} and P_M^{xyz}, respectively, then Formulas (1) and (2) are as follows.

$$P_M^{uvw} = (u_M, v_M, w_M) = u_M i_u + v_M j_v + w_M k_w, \quad (1)$$

$$P_M^{xyz} = (x_M, y_M, z_M) = x_M i_x + y_M j_y + z_M k_z. \quad (2)$$

In Formulas (1) and (2), i_u, j_v, and k_w are orthonormal basis of IMU base coordinate system. i_x, j_y, and k_z are orthonormal bases of the shoulder coordinate system. The position vector of fixed point M in the shoulder coordinate system is always P_M^{xyz}, while the projection of position vector P_M^{uvw} of this point in the IMU coordinate system in the directions of i_u, j_v, and k_w can be expressed as the following formula:

$$P_M^{uvw} = \& \begin{bmatrix} u_M \\ v_M \\ w_M \end{bmatrix} = \begin{bmatrix} i_u^T \left(u_M i_x + v_M j_y + w_M k_z \right) \\ i_v^T \left(u_M i_x + v_M j_y + w_M k_z \right) \\ i_w^T \left(u_M i_x + v_M j_y + w_M k_z \right) \end{bmatrix} = \begin{bmatrix} i_u^T i_x & i_u^T j_y & i_u^T k_z \\ j_v^T i_x & j_v^T j_y & j_v^T k_z \\ k_w^T i_x & k_w^T j_y & k_w^T k_z \end{bmatrix} \begin{bmatrix} x_M \\ y_M \\ z_M \end{bmatrix} = R \begin{bmatrix} x_M \\ y_M \\ z_M \end{bmatrix}. \quad (3)$$

According to the properties of rotation transformation, R is an orthogonal matrix; then, $R^{-1} = R^T$. R^T is the rotation transformation matrix.

The spatial position information of shoulder joint, namely, the relative relationship between shoulder coordinate system and IMU coordinate system, can be selected in the form of output data including Euler angle, quaternion, and rotation matrix. The attitude described by Euler angle is used in the research. Euler angles of IMU output are A_{roll}, A_{pitch}, and A_{yaw}, and its rotation matrix is the transformation matrix of shoulder coordinate system O_{xyz} and IMU coordinate system O_{uvw} [13]. By integrating the definition and IMU installation method, the real-time motion angle of healthy shoulder joint can be measured by IMU. The abduction and adduction angle of shoulder joint $\beta_1 = A_{\text{pitch}}$, the flexion and extension angle $\beta_2 = A_{\text{roll}}$, and the internal and external rotation angle $\beta_3 = A_{\text{yaw}}$.

3.2.2. Variable Domain Fuzzy Adaptive PD Control. Robot system is a complex nonlinear dynamic system with strong coupling. The traditional fuzzy proportional integral differential controller is only suitable for rough control occasions with fuzzy environment, and the fuzzy control effect is not ideal for high precision control problems. Therefore, variable domain fuzzy adaptive PD control is adopted in the system. On the premise that the rule form remains unchanged, the domain shrinks with the decrease of error, thus improving the control accuracy [14].

The input of the fuzzy adaptive PD controller in the variable domain adopted by the system is the change rate of the difference between the angle signal difference obtained from the trajectory of the shoulder joint of the limb and the difference. The initial fuzzy domain of the two values is divided into six levels, namely, $[-E3, -E2, -E1, -E0, E1, E2, E3]$ and $[-CE3, -CE2, -CE1, -CE0, CE1, CE2, CE3]$. The output of the fuzzy adaptive PD controller in the variable domain is the control moment of the robot τ_p. The domain of output torque can be expressed as $\tau_p = [-\tau_{p\ \min}, \tau_{p\ \max}]$. The fuzzy

producer is established through $\theta_e = [-E_{\min}, E_{\max}]$ and $d\theta_e/dt \in [CE_{\min}, CE_{\max}]$, as shown in the following formulas:

$$E = 6 \times \frac{(\theta_e - E_{\min})}{(E_{\max} - E_{\min})}, \tag{4}$$

$$CE = 6 \times \frac{(d\theta_e/dt - CE_{\min})}{(CE_{\max} - CE_{\min})}. \tag{5}$$

In Formulas (4) and (5), $E_{\min}$ and $E_{\max}$, respectively, represent the minimum and maximum values of angle signal difference θ_e domain. $CE_{\min}$ and $CE_{\max}$, respectively, represent the minimum and maximum values of angle signal difference change rate $d\theta_e/dt$ domain. E and CE are the output of fuzzy producer.

Fuzzy rules are designed according to the adaptive PD control rate as shown in the following formulas.

$$\tau_p = K_p E + K_d CE, \tag{6}$$

$$K_p = K_{p0} + \Delta K_p \times q_p, \tag{7}$$

$$K_d = K_{d0} + \Delta K_d \times q_d. \tag{8}$$

K_p and K_d are the final control parameters of PD controller. K_{p0} and K_{d0} are the initial setting parameters of PD controller. ΔK_p and ΔK_d are the output of fuzzy controller. And q_p and q_d are correction coefficients.

Fuzzy elimination of control is carried out through the membership maximum method, and the membership function peak value of the output fuzzy subset is directly selected as the determined value of the output. And the logical "union" of the output fuzzy subset τ_{pi} is $\tau_p = \bigvee_{l=1}^{6} \tau_{pi}$, and the exact output of the control variable τ_p is inverted by taking the median value [15]. Then, the domain of angle signal difference θ_e and its change rate $d\theta_e/dt$ can be gradually reduced, and the domain of reduced θ_e, $d\theta_e/dt$, and output torque τ_p can be determined, which can be expressed as follows:

$$E(t) = [-\alpha_1(t)E_{\min}, \alpha_1(t)E_{\max}], \tag{9}$$

$$CE(t) = [-\alpha_2(t)CE_{\min}, \alpha_2(t)CE_{\max}], \tag{10}$$

$$\tau_p(t) = \left[-\beta(t)\tau_{p\ \min}, \beta(t)\tau_{p\ \max}\right]. \tag{11}$$

In Formulas (9)–(11), $\alpha_1(t)$, $\alpha_2(t)$, and $\beta(t)$ are expansion factors of corresponding domains.

3.2.3. Muscle Strength Estimation of Affected Limb Based on sEMG. The noninvasive sEMG was adopted by the Delsy surface myoelectrometer, which was simple in form and did no harm to the subjects. Flexion/extension, abduction/adduction, and internal rotation/external rotation were used as arm motion patterns in mirror rehabilitation training. Referring to the relevant muscle contraction during shoulder joint motion, combined with the human anatomical structure, the most relevant muscles, anterior deltoid muscle, posterior deltoid muscle, middle deltoid muscle, and trapezius muscle, were selected, and the surface EMG sensor was worn at the corresponding muscle position.

In order to complete the muscle force estimation based on sEMG, force signals in the process of muscle force generation at the shoulder joint should be collected as reference data. In the research, ROBOTIQ FT300 six-dimensional force sensor was used for collection. In order to facilitate subsequent experiments, the force sensor used its own software for gravity compensation. During the experiment, the force sensor was placed on the part used to fix the affected limb in the robot component 3. During this process, sEMG (represented by X) and force signals (represented by F) of the four parts of the shoulder joint of the subject were collected in real time. For sEMG, the time-domain method for feature extraction was adopted to obtain the feature matrix X_F. And X_F and F were formed the sample S_m. The long short-term memory network (LSTM) performed the nonlinear mapping of the input network X_F to obtain the estimated value of the subject's shoulder joint force [16], as shown in the following formulas.

$$X = \begin{bmatrix} X_1 \\ X_2 \\ X_3 \\ X_4 \end{bmatrix} = \begin{bmatrix} x_{11}\, x_{12}\ \cdots x_{1m} \\ x_{21}\, x_{22}\ \cdots x_{2m} \\ x_{31}\, x_{32}\ \cdots x_{3m} \\ x_{41}\, x_{42}\ \cdots x_{4m} \end{bmatrix}, \tag{12}$$

$$F = \begin{bmatrix} F_x \\ F_y \\ F_z \end{bmatrix} = \begin{bmatrix} f_{x1} f_{x2}\ \cdots f_{xm} \\ f_{y1} f_{y2}\ \cdots f_{ym} \\ f_{z1} f_{z2}\ \cdots f_{zm} \end{bmatrix}, \tag{13}$$

$$S_m = \begin{bmatrix} X_F \\ F \end{bmatrix}. \tag{14}$$

In Formulas (12)–(14), $X_1 \sim X_4$ are the four channels of sEMG collected by the first to the fourth EMG sensor. F_x, F_y, and F_z are the force signals detected by the force sensor in the x, y, and z directions, respectively, and m is the number of sampling points.

The sEMG and force signals were collected by EMG sensors and force sensors, and muscle force estimation of affected limbs was completed through recurrent neural network (RNN) training. Traditional RNN had a dependency problem, but LSTM was a recurrent neural network. It could effectively fit the time-varying characteristics of sEMG of human body. Therefore, the system substituted the collected sEMG eigenvalues and force signals into LSTM to identify the muscle force of the affected limb [17]. In LSTM network, the selection of output action mainly consists of three stages. The first is the forgetting stage, in which the calculated Z_f is used as the forgetting gate to control the state S_{t-1} that needs to be forgotten and remembered in the previous state C_{t-1}. The second is the selective memory stage, in which the input S_t is selectively remembered. If a higher reward value can be obtained, it will be recorded; otherwise, it will be remembered less. Since RNN is sequential, the current input content is the state of

the current moment, and Z_i is used as the gating signal to control the selection. The third is the output stage. Z_0 is used to control which will be regarded as the output action of the current state. Meanwhile, tanh activation function is used to scale the C_{t-1} obtained in the previous stage [18]. Here, force signals obtained synchronously in the process of force generation of shoulder joint muscles and sEMG characteristic values of shoulder muscles were input as training samples of LSTM to train LSTM. Then, the force signal of shoulder joint muscle in the process of force generation was used as LSTM training sample to test the established muscle force estimation model. The trained LSTM could estimate the joint force output by sEMG eigenvalue and obtain the torque according to the distance from the force sensor to the shoulder joint.

3.2.4. Assisted Adaptive Adjustment of Affected Limb. The motion trajectory of the healthy limb captured by IMU in Section 3.2.1 was used as the mirror expected trajectory followed by the affected limb in mirror training, and the shoulder dynamic model was established through the healthy arm with length l and mass m. The shoulder angle collected by IMU in real time is θ_d, so the kinetic energy E_1 and potential energy E_2 of this system could be obtained, which could be expressed as $E_1 = 1/2ml^2\theta_d^2$ and $E_2 = mgl \sin\theta_d$, where g is the acceleration of gravity.

According to Lagrange equation, the following formula can be obtained.

$$\frac{d}{dt}\left(\frac{\partial L}{\partial \dot{\theta}_d}\right) - \frac{\partial L}{\partial \theta_d} = \tau_a, \tag{15}$$

In Formula (15), $L = E_1 - E_2$, and τ_a is the expected torque of shoulder joint movement following the healthy limb. The kinematic model of shoulder joint can be written in matrix form by Lagrange equation, which can be expressed as the following formula:

$$\tau_a = M(\theta_d)\ddot{\theta}_d + V\left(\theta_d, \dot{\theta}_d\right) + G(\theta_d). \tag{16}$$

In Formula (16), $M(\theta_d) = \begin{bmatrix} m & -ml\sin\theta_d \\ -ml\sin\theta_d & ml^2 \end{bmatrix}$ is inertial matrix. $V(\theta_d, \dot{\theta}_d) = \begin{bmatrix} 0 & -ml\dot{\theta}_d\cos\theta_d \\ 0 & 0 \end{bmatrix}\dot{\theta}_d$ is centrifugal force and Coriolis force vector. $G(\theta_d) = \begin{bmatrix} 0 \\ mgl\cos\theta_d \end{bmatrix}$ is the gravity vector. The difference between the expected torque of the affected limb τ_a following the healthy limb and the force torque of the affected limb τ_s is defined as the torque τ_d that the rehabilitation robot needs to compensate for the affected limb. At the same time, a gravity compensation link is introduced, and the gravity compensation torque is τ_G. Finally, the total joint torque of the rehabilitation robot is the torque sum of fuzzy adaptive PD control in variable domain, power compensation, and gravity compensation of the affected limb, as shown in the following formula:

$$\tau = \tau_p + \tau_d + \tau_G. \tag{17}$$

4. Result Analysis

4.1. Shoulder Joint Force Estimation Experiment. In the shoulder joint force estimation experiment, the exoskeleton-type shoulder joint rehabilitation robot was taken as the experimental platform and a healthy subject was selected. The right upper limb of the subject was simulated to wear the rehabilitation robot. In the fixed mode, the six-dimensional force sensor is fixed to the robot, and the sEMG acquisition device was worn at the corresponding muscle position of the affected limb. The force signal and sEMG of shoulder muscle were obtained synchronously. The sampling frequency of sEMG acquisition device was set at 2,000 Hz, and the sampling time (the time for performing sagittal forward flexion or backward extension and horizontal forward flexion or backward extension, respectively) was set at 30 s to collect sEMG signals of shoulder joint motion-related muscles during the above two groups of force movements. The mean absolute value (MAV) was used to extract the EMG eigenvalues. Zero calibration was carried out before the force sensor was used to collect shoulder joint force signals [19].

The affected limb of the subject made force movements in four directions of sagittal flexion or extension and horizontal flexion or extension by means of the shoulder, respectively, in the positive or negative direction and the positive or negative direction of the stress sensing axis. The sEMG and force signals in the process of shoulder joint movement were collected, and these two signals were input as the training samples of LSTM. After the training, LSTM estimated the output of shoulder joint force through sEMG eigenvalues.

The subjects were instructed to extend the affected limb to the side of the body as the initial position. The rehabilitation robot assisted the affected limb to perform the force action of sagittal extension and then back to the initial position and sagittal flexion and then back to the initial position. Namely, the sagittal flexion or extension was completed. The subject was instructed to raise the affected limb at the straight side as the initial position, and the rehabilitation robot assisted the affected limb to perform the force action of horizontal forward flexion and then back to the initial position and horizontal backward extension and then back to the initial position. Namely, the horizontal forward flexion or backward extension was completed [20]. The sagittal front flexion or extension and horizontal front flexion or extension groups were repeated 20 times. 10 times were selected as the training samples, and the remaining 10 times were used as the test samples. Figures 2(a) and 2(b) show sEMG and force signals measured when subjects performed the above two sets of movements. Figures 3(a) and 3(b) show the experimental results of shoulder joint force estimation of the subjects.

The solid line in Figure 3 represents the muscle force of shoulder joint of affected limb measured by the six-dimensional force sensor, which is the actual value. The dashed line represents the muscle force estimated by sEMG characteristic information, which is the estimated value. In Figure 3(a), the subject was instructed to perform 6 and 20

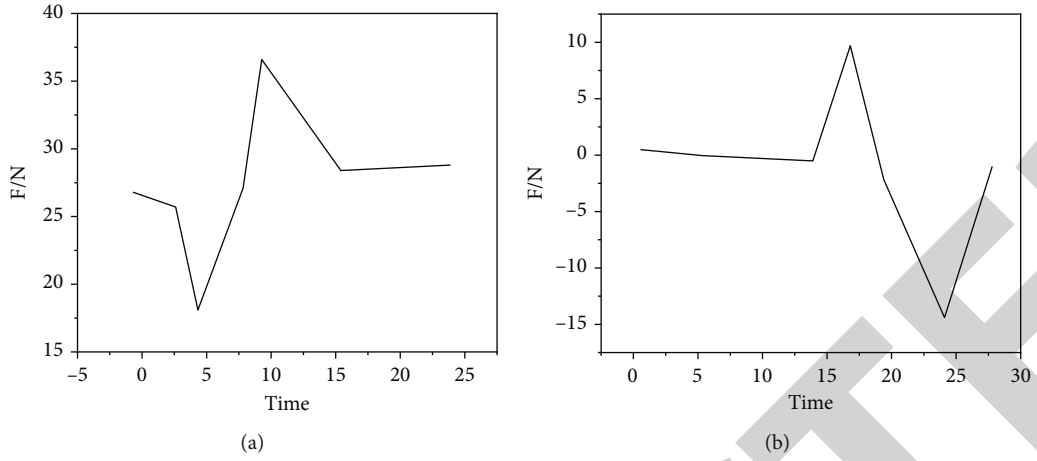

Figure 2: (a) sEMG and force signal of shoulder joint. (b) sEMG and force signal of shoulder joint.

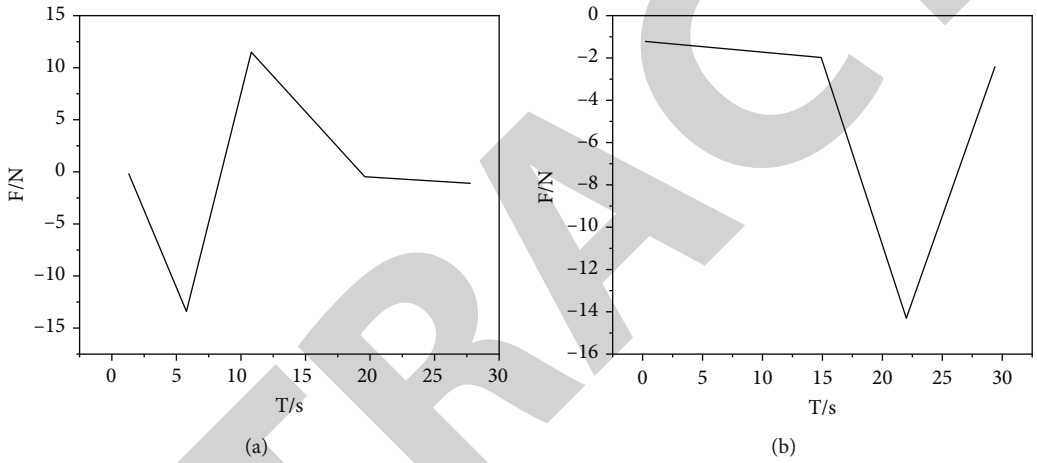

Figure 3: (a) Estimation of sagittal forward flexion or backward extension force of shoulder joint. (b) Estimation of sagittal forward flexion or backward extension force of shoulder joint.

sagittal forward flexion or backward extension movements of shoulder joint, respectively, for force estimation. Taking 20 repeated force movements as an example, it could be divided into four stages. (1) Initial position—sagittal backward extension. Within 2.9~4.8 s, the muscle strength of the affected limb increased in the opposite direction after sagittal backward extension from the initial position. (2) Sagittal backward extension—initial position. Within 4.8~7.5 s, the muscle strength of the affected limb decreased in the opposite direction when the subject underwent the force movement of sagittal backward extension back to the initial position. (3) Initial position—sagittal forward flexion. Within 7.5-11.4 s, the affected limb performed sagittal forward flexion from the initial position, and the muscle strength of the affected limb increased in the positive direction. (4) Sagittal forward flexion—initial position. Within 11.4~12.4 s, the positive direction of the muscle strength of the affected limb decreased when the subject underwent the force movement of sagittal backward extension back to the initial position. The root mean square (RMS) and mean absolute value of the error (MAVE) of the force measured in the sagittal flexion or extension direction of the shoulder joint during the four stages were calculated, with 0.76 N and 0.28 N, respectively. By comparing the error between the estimated value and the actual value of the specified force action performed for 6 times and 20 times, respectively, it could be seen that the error after 20 times of repeated test was significantly less than that after 6 times of repeated test, indicating that the trained LSTM network could accurately estimate the real distance of the affected limb [21]. Figure 3(b) shows that the subject was instructed to perform 6 and 20 sagittal forward flexion or backward extension movements of shoulder joint, respectively, for force estimation. Similarly, 20 repetitions of force movement were also taken as an example and divided into four stages. (1) Initial position—horizontal forward flexion. Within 14.2~16.3 s, the affected limb performed horizontal forward flexion from the initial position, and the muscle strength of the affected limb increased in the positive direction. (2) Horizontal forward flexion—initial position. Within 16.3~19.8 s, the affected limb returned to the initial position and the positive direction of muscle force decreased. (3) Initial position—horizontal backward extension. Within 19.8 to 22.6 s, the muscle strength of the affected limb increased in the opposite direction when the subject performed horizontal backward extension from

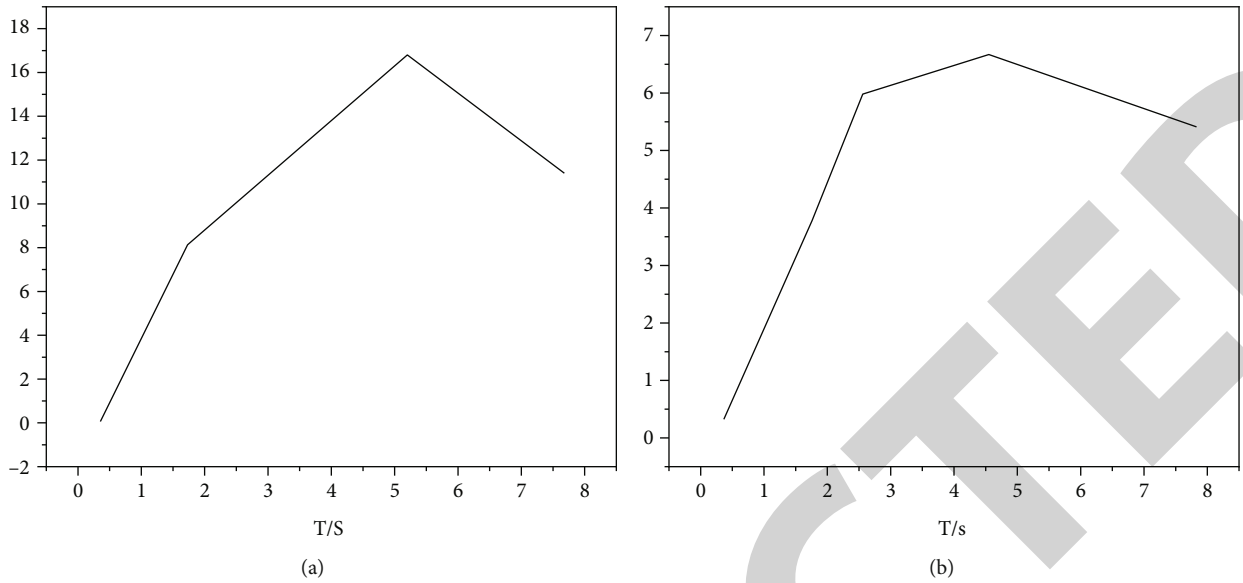

Figure 4: (a) Direction torque in sagittal forward flexion of shoulder joint. (b) Direction torque in sagittal backward extension of shoulder joint.

the initial position. (4) Horizontal backward extension—initial position. Within 22.6-24.9 s, the muscle strength of the affected limb decreased in the opposite direction when the subject performed the force movement of horizontal backward extension back to the initial position. In these four stages, RMS and MAVE of the measured force of shoulder joint in horizontal forward flexion or backward extension direction were 0.79 N and 0.41 N, respectively. By comparing the errors between the estimated values and the actual values of the 6 and 20 times force movements, respectively, it could also be seen that the errors after the 20 repeated tests were significantly less than the 6 repeated tests, indicating that the trained LSTM network could accurately estimate the real distance of the affected limb. The above results showed that the RMS and MAVE of the calculated force and measured value in the direction of sagittal forward flexion or backward extension and horizontal forward flexion or backward extension of shoulder joint were not greater than 1 N. Combined with the actual value and estimated value curves of Figures 3(a) and 3(b), it could be seen that the shoulder force output estimated by sEMG eigenvalue could better reflect the real shoulder muscle force measured by force sensor.

4.2. Mirror Rehabilitation Training Experiment. Similarly, in the mirror rehabilitation training experiment, the exoskeleton-type shoulder rehabilitation robot was used as the experimental platform and the six-dimensional force sensor was fixed on the robot. Subject wore IMU on the left upper limb as a healthy limb, a rehabilitation robot on the right upper limb as a simulated affected limb, and a sEMG acquisition device. During this process, the sampling frequency of the sEMG acquisition device was set at 2,000 Hz, and the sampling time was 8 s when performing sagittal forward flexion and 5 s when performing horizontal backward extension. The sEMG signals of the shoulder joint of the affected limb were collected, and their characteristic values were extracted when performing sagittal forward flexion and horizontal backward extension. After the force sensor was zeroed, the force signal of shoulder joint of affected limb was collected. The subject was instructed to put his healthy limb and the affected limb straight to the side of the body as the starting position, and the healthy limb should keep as much speed as possible to do the sagittal forward flexion of the shoulder. The affected limb should follow the healthy limb to do the incomplete force in the mirror direction under the condition of no force or less force than the healthy limb, so as to complete the sagittal forward flexion of the healthy limbs. Similarly, the subject was instructed to raise the healthy limb and the affected limb flatly before unstretching as the starting position and the healthy limb as far as possible to do the force movement of horizontal backward extension of shoulder joint with the uniform speed. The affected limb followed the healthy limb to do incomplete force in the mirror direction under the condition of no force or less force than the healthy limb, so as to complete the horizontal backward extension experiment of the healthy limb [22].

In the process of the two groups of rehabilitation movements, IMU was used to collect the trajectory of the limb and substitute it into the shoulder dynamic model to obtain the torque of the limb τ_a. Then, the estimated moment of the affected limb τ_s could be obtained by synchronously collecting the sEMG and force signals of the affected limb and substituting them into the muscle force estimation model in Section 4.1. The difference between the two is the compensation moment τ_d that could be adjusted adaptively to the affected limb. Experimental results are shown in Figures 4(a) and 4(b) [23].

Figure 4(a) shows the variation curves of the healthy limb torque τ_a, the estimated torque of the affected limb τ_s, and compensated torque of the affected limb τ_d when the healthy limb performed sagittal forward flexion motion of shoulder

joint at the same time. It can be seen that the healthy limb torque τ_a is gradually enlarged to approach 9.8 N due to the need to overcome its own gravity. Because the affected limb follows the incomplete force in the mirror direction of the healthy limb, τ_s is the same as the direction of τ_a, but $|\tau_s| < |\tau_a|$, and τ_s increases gradually to 5.6 N. The compensation moment of the affected limb τ_d defined above varies with the change of τ_a and τ_s. τ_d gradually increases to 4.2 N. Figure 4(b) shows the variation curves of the healthy limb torque τ_a, the estimated torque of the affected limb τ_s, and compensated torque of the affected limb τ_d when the healthy limb performed horizontal backward extension motion of shoulder joint at the same time. Compared with the experiment results of the implementation of sagittal forward flexion of shoulder joint, the direction of the muscle force of the affected limb and the healthy limb is the same, but the torque is small. The experimental process of horizontal backward extension of shoulder joint can be divided into five stages. (1) Forward acceleration stage: Within 0~1.0 s, τ_a and τ_s increase in a positive direction. (2) Forward deceleration stage: Within 1.0-2.2 s, τ_a and τ_s decrease in a positive direction. (3) Constant velocity stage: Within 2.2~3.3 s, it remains constant. (4) Reverse acceleration stage: Within 3.3~4.0 s, τ_a and τ_s increase in an opposite direction. (5) Reverse deceleration stage: Within 4.0~5.0 s, τ_a and τ_s decrease in an opposite direction. In these five stages, the compensation moment of the affected limb τ_d remains within −1.9~1.8 N with the change of τ_a and τ_s.

Through the above experiments, the adaptive compensation moment of the affected limb was obtained when the subject performed the sagittal forward flexion and horizontal backward extension of the shoulder joint, and the data were fed back to the shoulder rehabilitation robot in real time, so as to assist the affected limb to follow the healthy limb to perform the force action in the mirror direction. In this experiment, the sagittal forward flexion and horizontal backward extension of shoulder joints were repeated for 10 times, respectively. Through the movement trajectory of the healthy limb collected by IMU, the following trajectory of the affected limb was obtained by the mirror mapping [24, 25].

5. Conclusions

Aiming at shoulder rehabilitation patients, a mirror rehabilitation training system with adaptive adjustment power and its control algorithm was designed in the research, realizing the synchronous mirror movement between the rehabilitation robot assisted the affected limb and the healthy limb. The selected rehabilitation actions were shoulder sagittal flexion and horizontal extension. IMU and sEMG data of the healthy limb were collected during the rehabilitation process. The following trajectory of the affected limb was roughly consistent with that of the healthy limb, indicating that the rehabilitation effect of the affected limb was better due to the mirror rehabilitation training. By adding fuzzy adaptive PD control in variable domain, the difference between the estimated torque of the healthy limb and the affected limb was taken as the compensation torque of the affected limb, so as to realize the adaptive power compensation of the affected limb. By considering the recovery of the affected limb, the system gave full play to the training initiative of the affected limb and the rehabilitation training effect was better.

Data Availability

The data used to support the findings of this study are available from the corresponding author upon request.

Conflicts of Interest

The authors declare that they have no conflicts of interest.

References

[1] L. Yao, R. Dimitrakopoulos, and M. Gamache, "Training image free high-order stochastic simulation based on aggregated kernel statistics," *Mathematical Geosciences*, vol. 53, no. 7, pp. 1469–1489, 2021.

[2] Z. Zheng, Y. Liu, M. He, D. Chen, L. Sun, and F. Zhu, "Effective band selection of hyperspectral image by an attention mechanism-based convolutional network," *RSC Advances*, vol. 12, no. 14, pp. 8750–8759, 2022.

[3] D. Karimi and S. E. Salcudean, "Reducing the Hausdorff distance in medical image segmentation with convolutional neural networks," *IEEE Transactions on Medical Imaging*, vol. 39, no. 2, pp. 499–513, 2020.

[4] F. A. Baothman and B. S. Edhah, "Toward agent-based LSB image steganography system," *Journal of Intelligent Systems*, vol. 30, no. 1, pp. 903–919, 2021.

[5] S. Medghalchi, C. F. Kusche, E. Karimi, U. Kerzel, and S. Korte-Kerzel, "Damage analysis in dual-phase steel using deep learning: transfer from uniaxial to biaxial straining conditions by image data augmentation," *JOM*, vol. 72, no. 12, pp. 4420–4430, 2020.

[6] N. Yang, H. Tang, J. Yue, X. Yang, and Z. Xu, "Accelerating the training process of convolutional neural networks for image classification by dropping training samples out," *IEEE Access*, vol. 8, pp. 142393–142403, 2020.

[7] B. Loflin, K. Cluff, J. Griffith, and N. Mohammed, "Identification of shoulder joint clearance in space suit using electromagnetic resonant spiral proximity sensor for injury prevention," *Acta Astronautica*, vol. 170, pp. 46–54, 2020.

[8] C. Tsoi, C. Tsai, E. Law, R. Lee, and J. F. Griffith, "A comparison of ultrasound-guided rotator interval and posterior glenohumeral injection techniques for MR shoulder arthrography," *Clinical Imaging*, vol. 69, pp. 255–260, 2021.

[9] F. J. Liu, Z. Y. Sun, Y. F. Tuo, Y. Ji, and Y. X. Bai, "Effect of shoulder geometry and clamping on microstructure evolution and mechanical properties of ultra-thin friction stir-welded Al6061-T6 plates," *The International Journal of Advanced Manufacturing Technology*, vol. 106, no. 3-4, pp. 1465–1476, 2020.

[10] B. Vicharapu, H. Liu, H. Fujii, K. Narasaki, N. Ma, and A. De, "Probing residual stresses in stationary shoulder friction stir welding process," *International Journal of Advanced Manufacturing Technology*, vol. 106, no. 5-6, pp. 1573–1586, 2020.

[11] Y. Liu, X. Li, A. Zhu, Z. Zheng, and H. Zhu, "Design and evaluation of a surface electromyography-controlled lightweight upper arm exoskeleton rehabilitation robot," *International Journal of Advanced Robotic Systems*, vol. 18, no. 3, pp. 172988142110034–172988142110232, 2021.

[12] X. Li, Z. Zhu, N. Shen, W. Dai, and Y. Hu, "Deeply feature learning by CMAC network for manipulating rehabilitation robots," *Future Generation Computer Systems*, vol. 121, no. 1, pp. 19–24, 2021.

[13] M. Assad-Uz-Zaman, M. R. Islam, M. H. Rahman, Y. C. Wang, and E. Mcgonigle, "Kinect controlled NAO robot for telerehabilitation," *Journal of Intelligent Systems*, vol. 30, no. 1, pp. 224–239, 2021.

[14] G. Chen, Z. Mao, H. Zhou, and P. Yang, "Design and control strategy of 3-prismatic-revolute-spherical ankle rehabilitation robot," *Australian Journal of Mechanical Engineering*, vol. 8, pp. 1–14, 2021.

[15] S. Liao, H. Bao, T. Zhang, J. Liu, and L. Liu, "Integrated optical power splitter with continuously adjustable power splitting ratio," *IEEE Photonics Journal*, vol. 12, no. 6, pp. 1–13, 2020.

[16] X. Lin, Y. Peng, R. Hong, and Y. Wang, "Research on a novel discrete adjustable radiuses type continuously variable transmission," *Meccanica*, vol. 57, no. 5, pp. 1155–1171, 2022.

[17] Z. Zhang and H. Pang, "Continuously adjustable capacitor for multiple-pickup wireless power transfer under single-power-induced energy field," *IEEE Transactions on Industrial Electronics*, vol. 67, no. 8, pp. 6418–6427, 2020.

[18] A. Jafari, M. S. Nikoo, F. Karakaya, and E. Matioli, "Enhanced dab for efficiency preservation using adjustable-tap high-frequency transformer," *IEEE Transactions on Power Electronics*, vol. 35, no. 7, pp. 6673–6677, 2020.

[19] S. Mao, J. Li, A. Guo, T. Zhao, and J. Zhang, "An active multi-electrode array for collecting surface electromyogram signals using a-IGZO TFT technology on polyimide substrate," *IEEE Transactions on Electron Devices, PP*, vol. 67, no. 4, pp. 1613–1618, 2020.

[20] R. Gupta, I. S. Dhindsa, and R. Agarwal, "Surface electromyogram feature set optimization for lower limb activity classification," *IETE Journal of Research*, vol. 4, pp. 1–15, 2021.

[21] M. Fan and A. Sharma, *Design and implementation of construction cost prediction model based on SVM and LSSVM in industries 4.0. International Journal of Intelligent Computing and Cybernetics*, 2021.

[22] J. Jayakumar, S. Chacko, and P. Ajay, "Conceptual implementation of artificial intelligent based E-mobility controller in smart city environment," *Wireless Communications and Mobile Computing*, vol. 2021, 8 pages, 2021.

[23] L. Le, D. Yongfa, and L. Xin, "Ce-Mn mixed oxides supported on glass-fiber for low-temperature selective catalytic reduction of NO with NH_3," *Journal of Rare Earths*, vol. 32, no. 5, pp. 409–415, 2014.

[24] P. Ajay, B. Nagaraj, R. A. Kumar, R. Huang, and P. Ananthi, "Unsupervised hyperspectral microscopic image segmentation using deep embedded clustering algorithm," *Scanning*, vol. 2022, Article ID 1200860, 9 pages, 2022.

[25] G. Veselov, A. Tselykh, A. Sharma, and R. Huang, "Special issue on applications of artificial intelligence in evolution of smart cities and societies," *Informatica (Slovenia)*, vol. 45, no. 5, p. 603, http://www.informatica.si/index.php/informatica/article/view/3600.